Deformation Mechanism of Poly(ethylene terephthalate) Film under Uniaxial Stretching

Masaru Matsuo,* Minoru Tamada,† Takako Terada,‡ Chie Sawatari, and Masako Niwa

Department of Clothing Science, Faculty of Home Economics, Nara Women's University, Nara 630, Japan. *Received February 24, 1982*

ABSTRACT: The deformation of poly(ethylene terephthalate) was investigated by means of X-ray diffraction and small-angle light scattering techniques. The results showed that the deformation mechanism depends on the crystallinity of the specimen in the undeformed state. When a specimen with about 43% crystallinity was stretched, the crystallite orientation and the superstructural deformation were similar to those of a typical crystalline polymer such as polyethylene. That is, the crystal fiber axes were found to orient predominantly in the direction of stretching as assessed in terms of the second-order orientation factor, while the deformation of the superstructure was well accounted for by an affine deformation mode as shown by the good agreement between the experimental and theoretical results of H_v scattering patterns. On the other hand, when an amorphous specimen with about 3% crystallinity was stretched, the scattering showed a broad four-leaf lobe pattern at small azimuthal angles and a sharp narrow four-leaf streak pattern at large azimuthal angles. This behavior was analyzed by assuming the existence of a row-nucleated sheaflike structure whose rows are preferentially oriented at a particular angle with respect to the stretching direction. In this analysis, the *H*-function proposed by Hoseman was used as a probability of finding the nearest-neighbor particle at a displacement vector. The calculated pattern was rather close to the observed one. This agreement implies that the row-nucleated sheaflike texture arises with lamellar overgrowth where the rows are preferentially oriented at a particular angle with respect to the stretching direction.

I. Introduction

The morphology and deformation of poly(ethylene terephthalate) (PET) under uniaxial stretching are of interest because wide variations in crystallinity are easily accomplished and maintained. Extensive work has been reported on the study of the orientation of both crystalline and amorphous regions as well as of the deformation of the superstructure in regions in the process of strain-induced crystallization. The deformation mechanism has been studied by X-ray diffraction,[1-5] light scattering,[6-10] infrared,[2] and stress–strain[4] measurements. These investigations have provided a comprehensive view of the crystal and amorphous orientations[2-5] and the superstructural deformation mechanism[6-9] of PET films and fibers. Dumbleton and Bowles[5] estimated the orientation of the crystal fiber axis (the crystal *c* axis) from that of the ($\bar{1}05$) crystal plane, and Farrow and Bagley[3] used the average square of the orientation of the (100) and (010) crystal planes determined from the distribution of intensity of meridional reflections. On the other hand, Misra and Stein[9] investigated the difference of the deformation behavior of superstructures drawn below and above the glass transition temperature through careful observation of light scattering patterns.

This paper deals with the orientation behavior of crystalline and amorphous regions in relation to the deformation of superstructures within specimens having two different degrees of crystallinities, 43 and 3%, under uniaxial stretching. Quantitative estimation of the orientation behavior for the crystal fiber axes and the amorphous chain segments is carried out in terms of the second-order orientation factor. The orientation factor of the crystal fiber axes is obtained from that of five crystal planes. The orientation factor of amorphous chain segments is evaluated by subtracting the crystalline contribution from the total birefringence. The deformation of superstructures is studied by means of the light scattering technique. It is an objective of this experiment to investigate the crystallinity dependence of the deformation mechanism of PET films from two viewpoints. One is the molecular orientation and the other is the formation of the superstructure associated with the lamellar orientation mode under strain-induced crystallization.

II. Experimental Section

Samples were prepared from 350-μm amorphous PET films (about 3% crystallinity) obtained through the courtesy of the Film Division of Toray Industries, Inc., Siga. The density measured by a pycnometer, with a mixture of *n*-heptane and carbon tetrachloride as a medium, was found to be 1.338 g/cm^3. Elongation was done by using two kinds of specimens, the amorphous PET and the heat-treated PET (about 43% crystallinity). The heat-treated specimen was obtained by holding the amorphous PET for 4 h in a nitrogen atmosphere at 210 °C and then slowly cooling it to room temperature. This specimen was pretreated in a water bath at 90 °C for 30 min and stretched, so as to obtain uniform deformation without necking. The amorphous PET films were preheated at 95 °C for 15 min and stretched at the same temperature to the desired extension ratios without necking. The preheating time did not cause an increase of crystallinity, except an increase of crystallization occurred when the time was over 60 min. The degree of crystallinity was calculated by assuming the densities of the crystal and amorphous regions to be 1.455 and 1.335 g/cm^2,[11] respectively.

The orientation distribution functions of the reciprocal lattice vectors of the crystal planes were obtained by means of X-ray diffraction measurements at 100 mA and 40 kV with nickel-filtered Cu Kα radiation. In these measurements, the widths of the diverging, scattering, and receiving slits were $^1/_6$°, $^1/_6$°, and 0.15 mm, respectively. The X-ray diffraction measurements were carried out for the equatorial direction with respect to the crystal planes at a fixed value of θ_j, which denotes the polar angle between the stretching direction and the reciprocal lattice vector of the *j*th crystal plane. The changes of θ_j were carried out at appropriate intervals from 0 to 90°. The scanning speed with respect to the Bragg angle was $^1/_8$° min^{-1}. After corrections to the observed X-ray diffraction intensity (such as air scattering, background noise, polarization, and absorption) were applied and the contribution of the amorphous halo from the corrected total intensity curve was subtracted, the equatorial diffraction curve was obtained as a function of the Bragg angle $2\theta_B$. This intensity curve is believed to be due to the contribution of the diffraction intensity from the crystalline phase. The intensity curve may be separated into the contributions from the individual crystal planes on the assumption that each peak has a symmetric form given by a Lorenz function of $2\theta_B$.

† Yamagata University.
‡ Present address: Tamaki Women's College.

0024-9297/82/2215-0988$01.25/0

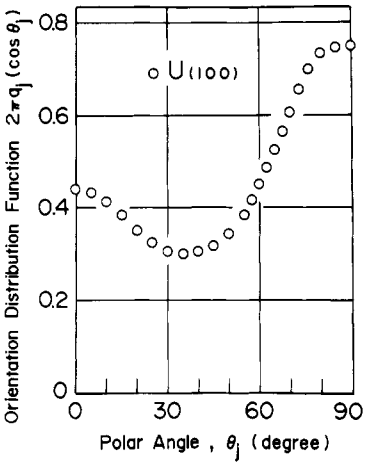

Figure 1. Orientation distribution function for the reciprocal lattice vector of the (100) crystal plane obtained from X-ray diffraction at the extension ratio of $\lambda = 2.0$.

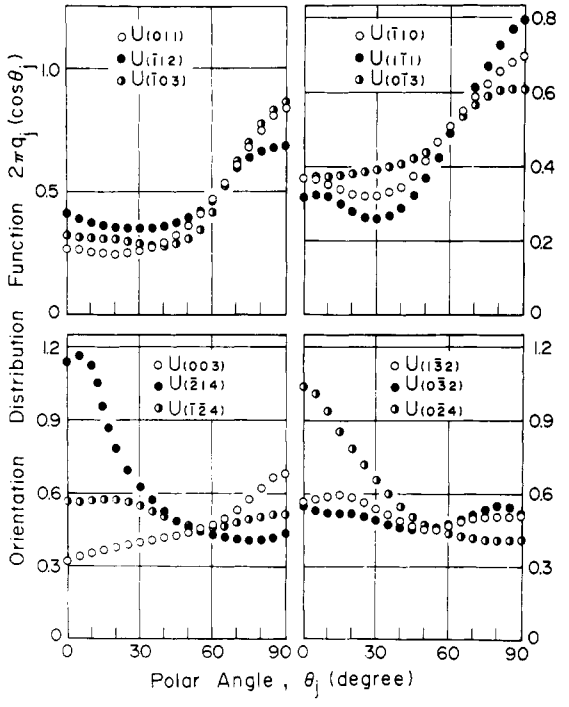

Figure 2. Orientation distribution functions for the reciprocal lattice vector of crystal planes obtained from X-ray diffraction at the extension ratio of $\lambda = 2.0$.

Light scattering patterns were obtained with a 3-mW He–Ne gas laser as a light source. Diffuse surfaces were avoided by sandwiching the specimens between the microcover glasses with silicone oil of an appropriate refractive index as immersion fluid.

III. Results and Discussion

We consider first the case of samples with a degree of crystallinity of 43%. Roe and Krigbaum[12-15] have proposed a method that is now widely used to characterize the distribution of crystallites in polymer specimens. Basically, the method involves the calculation of the orientation distribution function of the reciprocal lattice vectors using data from X-ray diffraction measurements. From this information the crystalline orientation function may be determined if the diffracted X-ray intensity from a sufficiently large number of crystal planes can be accurately measured.[13,15-17] We tried to apply this method to our stretched samples of PET. Figures 1–6 show the orientation distribution functions of the reciprocal lattice vectors of the crystal planes for the sample of 43% crystallinity. Unfortunately, these data are not sufficient to obtain the crystallite orientation function because except for the five crystal planes (100), (1̄10), (010), (11̄1), and (01̄1), the intensities of the reflections were too weak for accurate measurement. The number of crystal planes needed for application of this method increases with the complexity of the crystal unit cell, and in the case of triclinic PET at least 20 planes are required. For this reason we were forced to use an alternative procedure involving the estimation of the second-order orientation factor (F_{20}^j), which is given by the well-known expression

$$F_{20}^j = \tfrac{1}{2}(3\cos^2\theta_j - 1) \qquad (1)$$

where θ_j is the angle between the jth reciprocal lattice vector and the stretching direction. F_{20}^j characterizes the crystallite orientation distribution, with variation between $-\frac{1}{2}$ and 1. For random orientation of the jth axis, F_{20}^j is 0, while for complete orientation parallel and perpendicular to the stretching direction, F_{20}^j is unity and $-\frac{1}{2}$, respectively.

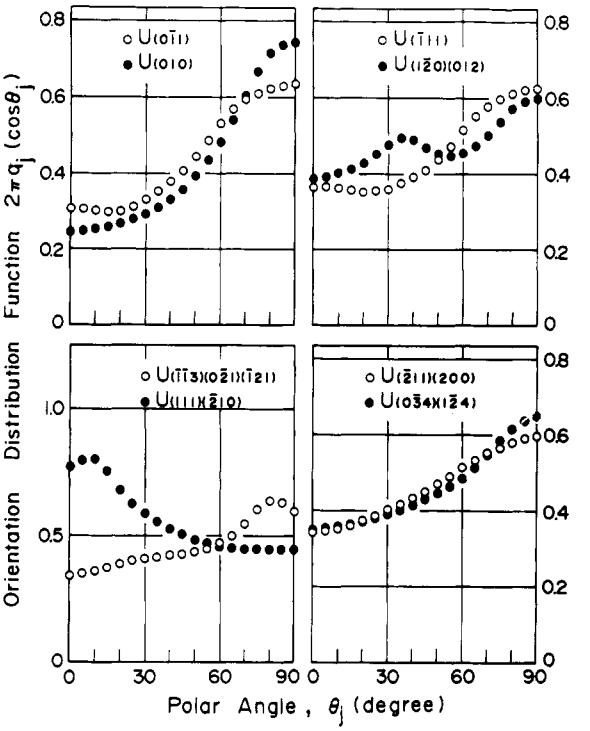

Figure 3. Orientation distribution functions for the reciprocal lattice vector of crystal planes obtained from X-ray diffraction at the extension ratio of $\lambda = 2.0$.

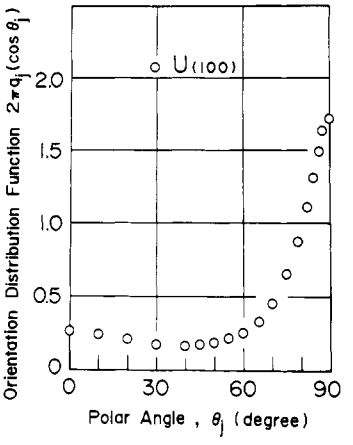

Figure 4. Orientation distribution function for the reciprocal lattice vector of the (100) crystal plane observed from X-ray diffraction at the extension ratio of $\lambda = 3.8$.

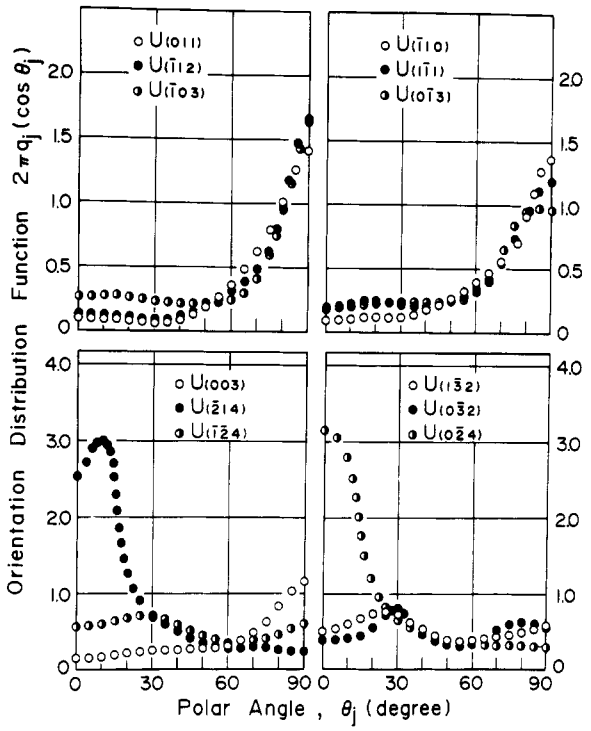

Figure 5. Orientation distribution functions of the reciprocal lattice vector of crystal planes observed from X-ray diffraction at the extension ratio of $\lambda = 3.8$.

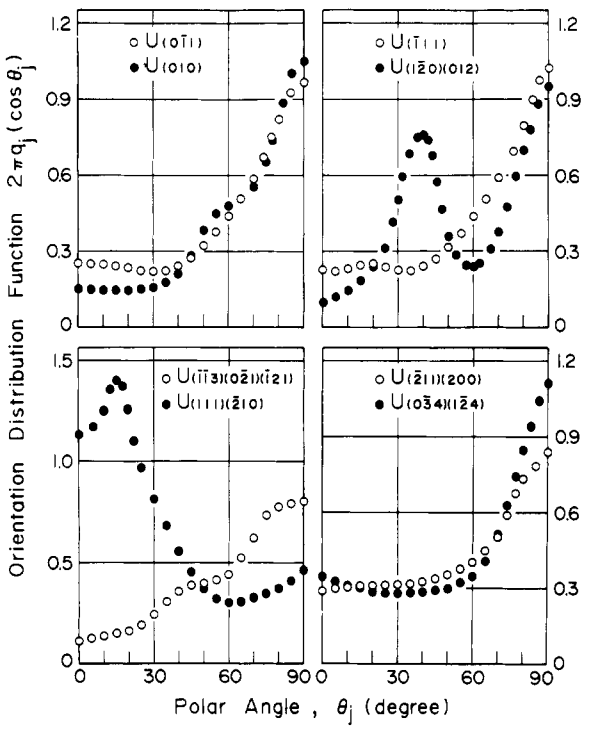

Figure 6. Orientation distribution functions for the reciprocal lattice vector of crystal planes obtained from X-ray diffraction at the extension ratio of $\lambda = 3.8$.

Table I
Direction of Coordinate Axes

coordinate system	direction of X_i, V_i, and U_i axes	
	$i = 1$	$i = 3$
O-$X_1X_2X_3$	normal to film surface	stretching direction of film specimen
O-$U_1U_2U_3$	crystal a^* axis of poly(ethylene terephthalate) crystallite	crystal c axis of poly(ethylene terephthalate) crystallite

Now, using a procedure described by Roe,[14] one can shown (see Appendix I) that the second-order orientation factor may also be expressed as follows:

$$F_{20}^{j} = F_{200}P_2(\cos\Theta_j) + \tfrac{1}{3}(F_{201}\cos\Phi_j - G_{201}\sin\Phi_j) \times P_2^1(\cos\Theta_j) + \tfrac{1}{12}(F_{202}\cos 2\Phi_j - G_{202}\sin 2\Phi_j)P_2^2(\cos\Theta_j) \quad (2)$$

where

$$P_2(x) = (1/2)(3\cos^2 x - 1) \quad (2a)$$

$$P_2^1(x) = 3(1 - x^2)^{1/2}x \quad (2b)$$

$$P_2^2(x) = 3(1 - x^2) \quad (2c)$$

Θ_j and Φ_j are the polar and azimuthal angles of the lattice vector U_j in the Cartesian coordinates O-$U_1U_2U_3$ of the structural unit. Table I shows the geometrical interrelation between the Cartesian systems of the structural unit O-$U_1U_2U_3$ and in the specimen O-$X_1X_2X_3$. Table II shows the values of Θ_j and Φ_j calculated from the unit cell parameters proposed by Daubeny et al.[11] By measuring the reciprocal lattice vectors for each of the five crystal planes (100), ($\bar{1}10$), (010), ($1\bar{1}1$), and ($0\bar{1}1$), the corresponding values of F_{20}^{j} were calculated from eq 1. Then substituting the values of F_{20}^{j} into eq 2 gives five sorts of simultaneous linear equations that can be solved to obtain the five unknown coefficients F_{200}, F_{201}, F_{202}, G_{201}, and G_{202}. Finally, with a knowledge of the values of these five

Table II
Crystallographic Parameters for the Five Plane Normals Contributing to the Measured Intensity

i	(hkl)	$2\theta_B$	Θ_j	Φ_j
1	$(0\bar{1}1)$	16.42	59.85	254.04
2	(010)	17.53	90.00	59.44
3	$(\bar{1}10)$	22.55	90.00	137.83
4	(100)	25.71	90.00	0.00
5	$(1\bar{1}1)$	27.85	72.66	300.56

coefficients, the orientation factors for the three principal crystallographic axes could be calculated.

Now we discuss the second-order orientation factor, F_{200}, of the amorphous chain segments. The contribution from the refractive index tensor n_{ij}^{co} of the crystallographic structural unit to the principal refractive tensor N_{ij}^{co} of the bulk material is given by

$$\langle N_{ij}^{co}\rangle = \sum_{k=1}^{3}\sum_{l=1}^{3} n_{ij}^{co}\langle t_{ki}t_{lj}\rangle \quad (3)$$

where t_{ki} is, for example, the direction cosine between the X_i axis and the U_k axis. n_{33}^{co} and n_{11}^{co} are the refractive indexes along the crystal c axis and along the crystal a^* axis corresponding to the direction normal to the benzene ring. n_{22}^{co} is the refractive index in the direction perpendicular to the crystal c and a^* axes. In order to obtain the tensor $\langle N_{ij}^{co}\rangle$, it is necessary to calculate the mean value of N_{ij}^{co} by taking the average of the orientation distribution function over all the orientations of the structural units. Considering the fiber texture of the bulk, the birefringence contribution of crystallites to bulk material may be estimated by assuming $n_{ij}^{co} = 0$ $(i \neq j)$ in eq 3 and is given by

$$\Delta_c = \langle N_{33}^{co}\rangle - \langle N_{22}^{co}\rangle \text{ (or } \langle N_{11}^{co}\rangle) = \{n_{33}^{co} - (1/2)(n_{11}^{co} + n_{22}^{co})\}F_{200} + (1/4)(n_{11}^{co} - n_{22}^{co})F_{202} \quad (4)$$

Table III
Second-Order Orientation Factor of the Three Principal Crystallographic Axes and Amorphous Chain Segments

extension ratio	a axis	b axis	c axis	amorphous chain segment
λ = 2.0	−0.027	−0.149	0.258	0.142
λ = 3.8	−0.245	−0.265	0.501	0.789

where F_{200} and F_{202} are as defined above. Assuming that the birefringence effect of the amorphous phase, Δ_{am}, may be estimated by subtracting[18] the crystalline contribution from the total birefringence, Δ_t, we have

$$\Delta_{am} = \frac{\Delta_t - X_c\Delta_c}{1 - X_c} \tag{5}$$

where X_c is the degree of volume crystallinity. Δ_{am} is given by

$$\Delta_{am} = \{n_{33}^{am} - \tfrac{1}{2}(n_{11}^{am} + n_{22}^{am})\}(F_{200}^{am})' \tag{6}$$

where the significance of the various parameters is discussed below.

The principal refractive index of the PET crystal is estimated in the usual way by assuming the atomic arrangements within the crystal reported by de Daubeny et al.[11] and the values of the bond polarizabilities according to Bunn and de Daubeny[19] and by neglecting the uncertain effect of the internal field within the crystal and of secondary bonds upon the principal polarizabilities. On the basis of the principal polarizabilities obtained by the above estimation, the principal indices are calculated by the Lorenz–Lorenz relation, which is given by Sakaguchi et al.[20] as follows:

$$n_{33}^{co} = 1.806$$
$$n_{22}^{co} = 1.733$$
$$n_{11}^{co} = 1.398 \tag{7}$$

The density of the crystal region is taken as 1.455 g/cm^3.

The refractive indices of the amorphous phase, assuming rotational ellipsoidal anisotropy around the a^* axis, are again estimated from the polarizabilities, the difference in density from that of the crystalline phase being taken into account. This procedure gives

$$n_{33}^{am} = 1.3615$$
$$n_{22}^{am} = n_{11}^{am} = 1.6874 \tag{8}$$

where n_{33}^{am} is the refractive index along the axis normal to the benzene ring and n_{22}^{am} and n_{11}^{am} are the refractive indices perpendicular to the above axis. The density of the amorphous region is taken as 1.335 g/cm^3. Hence, since $n_{33}^{am} < n_{22}^{am}$, $(F_{200}^{am})'$ corresponds to the second-order orientation factor of the a^* axes. In the case when the amorphous chain axes orient randomly around their own axes, the orientation factors of the other two axes perpendicular to the amorphous chain axis become equivalent with respect to the stretching direction. Then the orientation factor of the amorphous chain axes may be given as follows:

$$F_{200}^{am} = -2(F_{200}^{am})' \tag{9}$$

Table III presents the second-order orientation factors of the three principal crystallographic axes and amorphous chain segments. The values for the crystal c axes at λ = 2.0 indicate the preferential orientation to the stretching direction and this tendency becomes pronounced at λ = 3.8. The values for the crystal a axes at λ = 2.0 show almost random rotation, while the crystal b axes orient predominantly perpendicular to the stretching direction. However, the orientations of the crystal a and b axes at λ = 3.8 become almost the same, showing that these axes are preferentially oriented perpendicular to the stretching direction. This indicates the transformation of the PET structure from a deformed spherulitic to a fibrous texture. The amorphous chain segments at λ = 2.0 take a somewhat preferential orientation to the stretching direction but the degree of orientation is not as great as that of the crystal c axes. By contrast, the amorphous chain segments at λ = 3.8 attain very considerable preferential orientation and the orientational degree is much more pronounced than that of the crystal c axes.

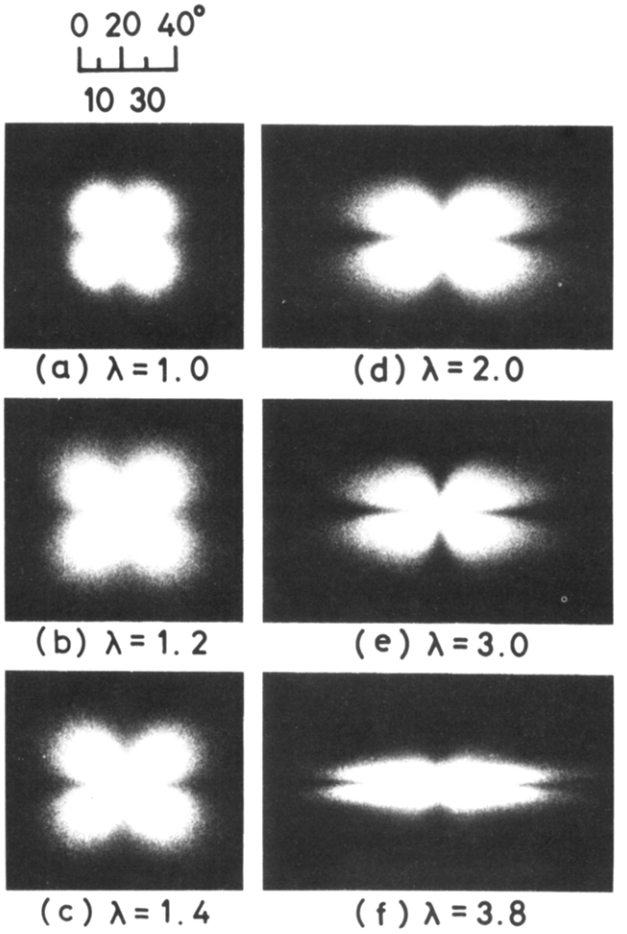

Figure 7. H_v light scattering patterns from the specimen with degree of crystallinity 43%. The stretching direction is vertical.

In order to obtain information on the deformation of the superstructure, we made low-angle light scattering measurements on the stretched specimens. Figures 7 and 8 show H_v and V_v light scattering patterns, respectively, at various extension ratios. The H_v scattering patterns at higher elongations have four lobes extended in the horizontal direction and show a maximum in the polar direction along the azimuthal angle of highest intensity. This is characteristic of the deformation of spherulitic textures. The V_v scattering patterns indicate that the optical axes are perpendicular to the spherulite radius.

Figure 9 shows the theoretical results of H_v scattering patterns calculated on the basis of a two-dimensional spherulitic model by assuming an affine deformation of the spherulite as well as an affine orientation of the optical axes. The theory does not distinguish between the crystalline and amorphous orientational components of the

Table IV
Dimensional Changes during the Drawing of PET Films

λ_3	1.2	1.5	1.7	2.0	2.3	2.5	2.7	3.0	3.5	3.8	4.0	4.5
λ_2	0.9120	0.8313	0.7653	0.7200	0.6880	0.6427	0.6140	0.5760	0.5333	0.4947	0.4873	0.4833
λ_1	0.9387	0.8395	0.7707	0.7029	0.6885	0.6608	0.6427	0.6373	0.5387	0.5367	0.5200	0.4773
$\lambda_3\lambda_2\lambda_1$	1.0273	1.0468	1.0027	1.0122	1.089	1.0617	1.0655	1.1013	1.0055	1.0106	1.0136	1.0381

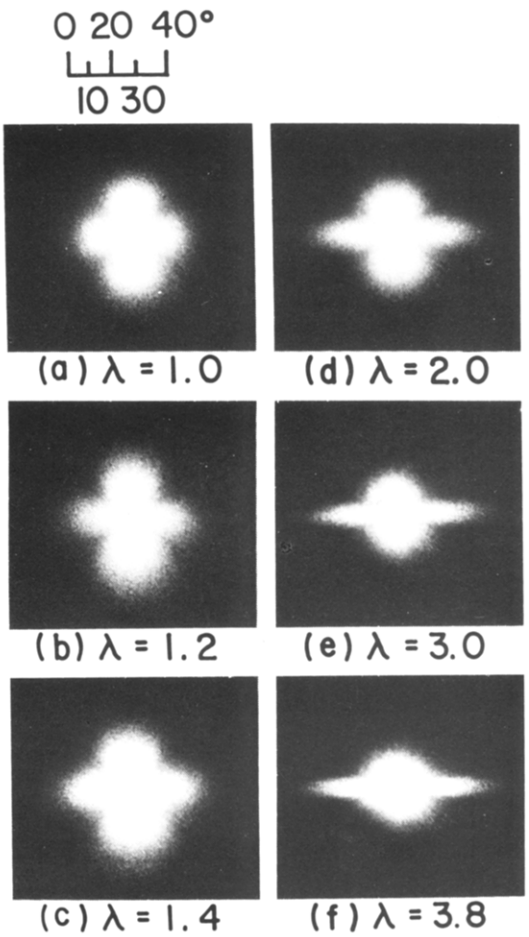

Figure 8. V_v light scattering patterns from the specimen with degreee of crystallinity 43%. The stretching direction is vertical.

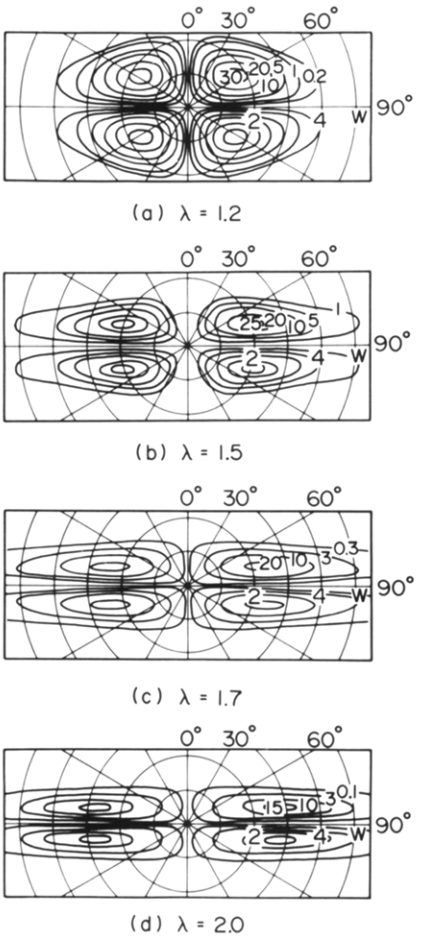

Figure 9. H_v light scattering patterns calculated by assuming an affine deformation model.

spherulite birefringence, which entails a limitation. The inclusion of the contributions from both of these birefringent sources would involve a fairly large number of parameters, the estimation of which would be difficult. Incidentally, detailed calculations for a three-dimensional spherulite were carried out by Samuels[21] and van Aartsen et al.[22] The former calculation[21] was carried out by introducing an affine deformation of a spherulitic volume, whereas the latter calculation[22] was made by introducing nonaffine orientation of the optical axes in addition to an affine deformation of a spherulitic volume. The latter treatment[22] is essentially the best to analyze deformation for small-size spherulites but is somewhat complicated in terms of mathematical description. Hence, in the present paper, the treatment for a two-dimensional model is adopted, as the two-dimensional treatment is not very different from the three-dimensional one. The calculation procedure is presented in Appendix II. The patterns observed in Figure 7 are well accounted for by the calculated results in Figure 9. It therefore seems reasonable to conclude that the mechanism of deformation of the spherulites in the drawn film corresponds to the assumptions made in the model. Judging from the results X-ray diffraction and light scattering measurements, the molecular orientation[16] and spherulitic deformation[23] are similar to those of a typical crystalline polymer such as polyethylene. We now consider the H_v scattering patterns of the amorphous PET films under uniaxial stretching.

Figures 10 and 11 show, respectively, the scattering patterns at low and high elongations of the amorphous (i.e., 3% crystallinity) PET films. The patterns in Figure 10 are elongated in the stretching direction and show a maximum in the polar angle direction along the azimuthal angle of highest intensity. Misra and Stein[9] have previously observed this phenomenon for PET films drawn above the glass transition temperature. They interpreted these patterns as being due to the scattering from sheaflike textures rather than ellipsoidal spherulites.

The pattern in Figure 11 shows four broad lobes at small azimuthal angles and four narrow streaks at large azimuthal angles. The question can be raised whether this multilobed pattern could be associated with a biaxial component of stretching that can arise from one-dimensional stretching of a sample of small length-to-width ratio. In this connection, Table IV shows the changes in three dimensions of the drawn sample, with the extension ratio λ_3 in the stretching direction, λ_2 in the transverse direction, and λ_1 in the thickness direction. The value of λ_1 is close to that of λ_2 and the product $\lambda_1\lambda_2\lambda_3$ becomes unity. This indicates that the deformation mode of the stretched sample is uniaxial. Accordingly, the multilobed patterns in Figure 11 cannot be associated with a biaxial component

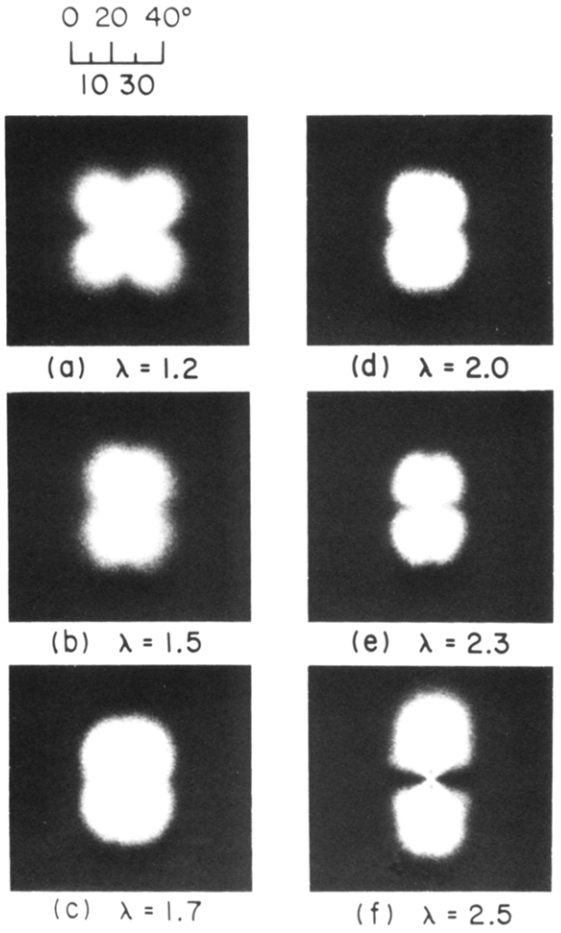

Figure 10. H_v light scattering patterns of amorphous PET films stretched to an extension ratio of λ = 2.5. The stretching direction is vertical.

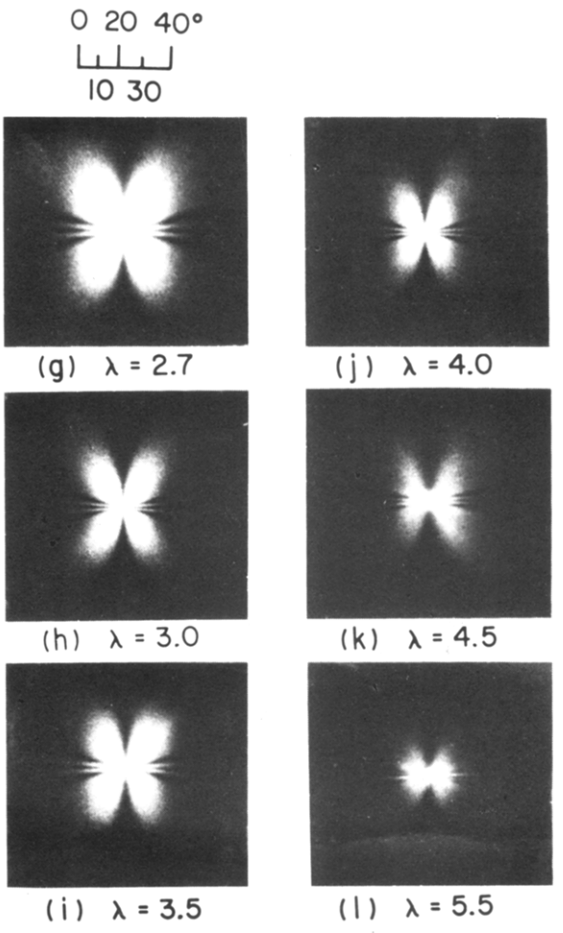

Figure 11. H_v light scattering patterns of amorphous PET films stretched to an extension ratio of λ = 5.5. The stretching direction is vertical.

of inner stress (or strain) due to one-dimensional stretching.

The change of the scattering patterns in Figure 10 and 11 is thought to be due to crystallization under uniaxial stretching and as such obviously reflects the growth of sheaflike superstructures[23,24] and their characteristic orientation with respect to the stretching direction. Figure 12 shows that the sharp narrow streaks at large azimuthal angles, as shown in Figure 11, are dependent upon the degree of crystallinity. The crystallinity is almost constant below an extension ratio of λ = 2.5, but it increases beyond this extension ratio. This critical extension ratio is connected with the appearance of the sharp narrow four-leaf pattern as streaks, and the change in slope between λ = 2.5 and λ = 2.7 is believed to be due to the effect of strain-induced crystallization.

It has been suggested above that the change in the scattering patterns during sample elongation is due to strain-induced crystallization. This should be accompanied by increased molecular orientation and there should be a corresponding increase in birefringence. In order to test this suggestion, we have measured the birefringence as a function of extension ratio. The results are shown in Figure 13. The birefringence shows a gradual linear increase at smaller strains up to λ = 3.0 and a considerable linear increase beyond λ = 3.0. This change in slope at around λ = 3.0 is associated with the crystallite orientation as well as the growth of crystallites. In order to verify the presumption discussed above, we obtained a wide-angle X-ray pattern for undrawn and drawn PET films as shown in Figure 14. Figure 14a shows a characteristic amorphous halo obtained from an unknown amorphous sample of

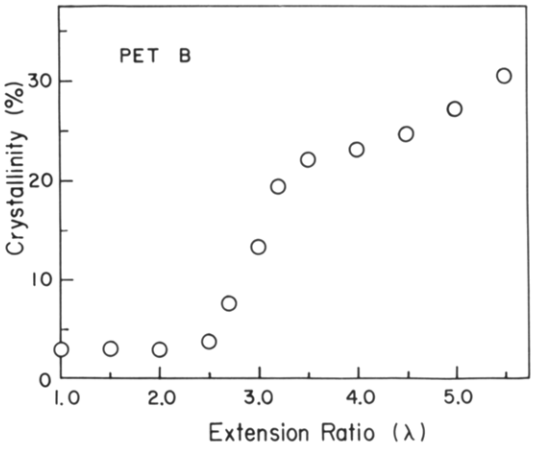

Figure 12. Crystallinity measured as a function of extension ratio.

PET preheated at 95 °C for 15 min. This amorphous halo was observed up to an extension ratio of λ = 2.5 and then assumes an ellipsoidal shape with the long axis in the equatorial direction. This behavior indicates the orientation of amorphous chain segments in the direction of stretching. This is in agreement with the gradual linear increase of birefringence up to about λ = 3.0 shown in Figure 13. Figure 14d is a diffraction pattern at λ = 3.0 and shows diffuse lobes in the equatorial direction. This indicates the existence of crystalline or semicrystalline material in the sample. With further increasing extension ratios, the diffraction pattern becomes clearly defined as arcs; this suggests that an increase of crystallinity and a higher orientation of crystals are attained in the samples.

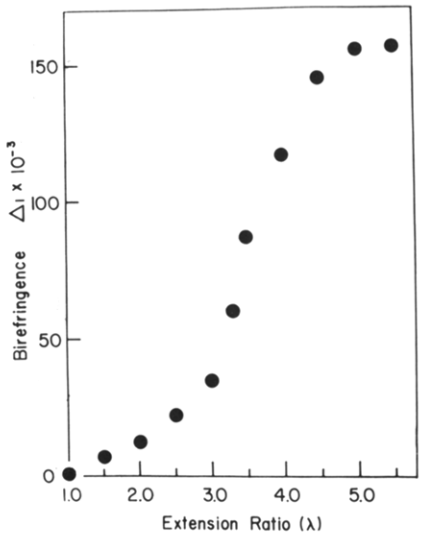

Figure 13. Birefringence measured as a function of extension ratio.

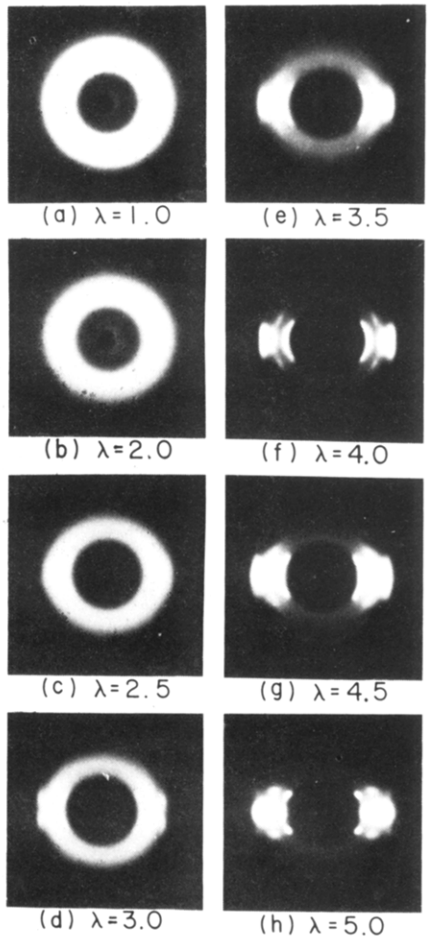

Figure 14. Wide-angle X-ray diffraction patterns for drawn amorphous PET. The stretching direction is vertical.

This is completely consistent with the considerable linear increase of birefringence in Figure 13 and the increase of crystallinity in Figure 12. The (010) and (100) crystal planes give diffraction lines in the equatorial regions, which indicates their preferred orientation parallel to the stretching direction. This tendency is similar to the orientation of the (100) and (010) crystal planes of the specimen at $\lambda = 3.8$ shown in Figures 4 and 6. Thus it is concluded that the crystal c axes are preferentially orientated in the direction of stretching. Unfortunately, the crystallite orientation cannot be evaluated in terms of the

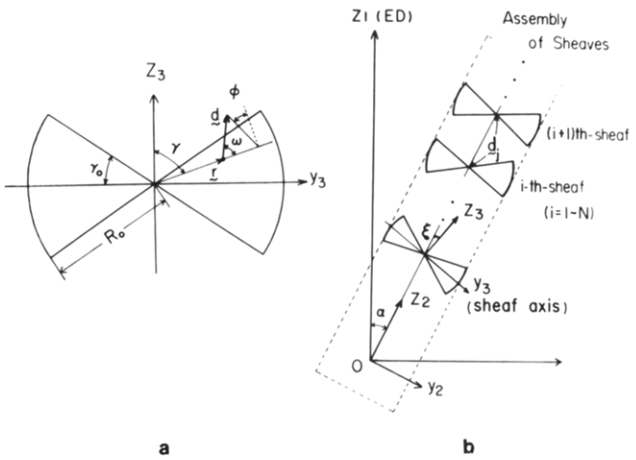

Figure 15. (a) Optically anisotropic sector as a model for the sheaflike texture. (b) Schematic diagram of assembly of sheaflike textures.

second-order orientation factor of the three crystallographic axes because of the weak X-ray diffraction intensity due to the low crystallinity of the sample.

Now considering again the scattering patterns in Figures 10 and 11, we may explain the sequence of deformation by the existence of a row-nucleated sheaflike superstructure whose rows are preferentially oriented at a particular angle ($\pm\alpha_0$) with respect to the stretching direction. The analysis of this kind of problem has already been carried out by Hashimoto et al.[25] using tubular-extruded poly(1-butene) films. They reported that the lamellar overgrowth from the nuclei gives a sheaflike crystalline superstructure aligned regularly along the nuclei and nearly side by side with their axes preferentially oriented perpendicular to the extrusion direction. In their report,[25] the depolarized and polarized components of scattered light from such an assembly of sheaves were analyzed in terms of a paracrystalline model of the Hoseman type.[26] We believe it is reasonable to adopt the method of Hashimoto et al.[25] to account for the change of the scattering patterns in Figures 10 and 11.

In order to facilitate understanding of the above concept, we refer to the schematic diagrams proposed in Figure 15. Efforts were made here to preserve the notation used by Hashimoto et al.[25] Figure 15a shows an idealized "fan" model for an isolated sheaflike superstructure.[27] The fan is composed of two identical opposite sectors with an aperture angle $2\gamma_0$ and radius R_0. The optical axis makes polar and azimuthal angles ω and β with the radius of the fan. Figure 15b shows a similar schematic diagram proposed by Hashimoto et al.[27] to account for the scattered intensity from the one-dimensional assembly of anisotropic sheaves. In this model system, if the assembly contains N particles and orients at an angle α with respect to the stretching direction, the scattered intensity $I(\mathbf{h},\alpha)$ may be given by

$$I(\mathbf{h},\alpha) = C\sum_j\sum_k \langle f_j f_k^* \exp\{-i(\mathbf{h}\cdot\mathbf{z}_{jk})\}\rangle \qquad (10)$$

where $\mathbf{z}_{jk}$ is a displacement vector between the jth and kth scattering centers and f^* denotes the complex conjugate of f. C is a constant. $\mathbf{h}$ is the scattering vector defined by

$$\mathbf{h} = (2\pi/\lambda)(\mathbf{s}_0 - \mathbf{s}') = (2\pi/\lambda)\mathbf{s} \qquad (11)$$

λ' is the wavelength of light in the medium, and the vectors $\mathbf{s}_0$ and $\mathbf{s}'$ are unit vectors along the propagation direction of the incident and scattered beams, respectively. If there is no orientation correlation between the individual par-

ticles and the orientation fluctuation is independent of the correlation in the position of the centers of each particle, eq 10 may be rewritten as follows:

$$I(\mathbf{h},\alpha) = C\{N\langle|f|^2\rangle + \langle|f|\rangle^2 \sum_{j\neq k}\sum \langle\exp\{-i(\mathbf{h}\cdot\mathbf{z}_{jk})\}\rangle\} \quad (12a)$$

$$I(\mathbf{h},\alpha) = C\{N[\langle|f|^2\rangle - |\langle f\rangle|^2] + |\langle f\rangle|^2[N + \sum_{j\neq k}\sum\langle\exp\{-i(\mathbf{h}\cdot\mathbf{z}_{jk})\}\rangle]\} \quad (12b)$$

The angular brackets denote an ensemble average, i.e., the average over all possible distributions of particles in the assembly with respect to the spatial distribution of scattering units and orientation of the individual particles. The double summation in eq 12 may be rewritten as follows:

$$\sum_{j\neq k}\sum\langle\exp\{-i(\mathbf{h}\cdot\mathbf{z}_{jk})\}\rangle = \sum_{j=1}^{N}[\sum_{k=1}^{j-1}\langle\exp\{-i(\mathbf{h}\cdot\mathbf{z}_{jk})\}\rangle + \sum_{k=j+1}^{N}\langle\exp\{-i(\mathbf{h}\cdot\mathbf{z}_{jk})\}\rangle] \quad (13)$$

As derived already by Hashimoto et al.,[25] the right-hand side of eq 13 is given by

$$I_1 = \sum_{k=1}^{j-1}\langle\exp\{-i(\mathbf{h}\cdot\mathbf{z}_{jk})\}\rangle = \sum_{k=1}^{j-1}\langle\prod_{i=k}^{j-1}\exp\{-(\mathbf{h}\cdot\mathbf{d}_i)\}\rangle = \sum_{k=1}^{j-1}\prod_{i=k}^{j-1}F(\mathbf{h}) = \sum_{k=1}^{j-1}F^{j-k} = (F - F^j)/(1 - F) \quad (14)$$

and similarly, the left-hand side of eq 13 is given by

$$I_2 = \sum_{k=j+1}^{N}\langle\exp\{-i(\mathbf{h}\cdot\mathbf{z}_{jk})\}\rangle = \sum_{k=j+1}^{N}\langle\prod_{i=j}^{k-1}\exp\{(\mathbf{h}\cdot\mathbf{d}_i)\}\rangle = \sum_{k=j+1}^{N}\prod_{i=j}^{k-1}F^*(\mathbf{h}) = \sum_{k=j+1}^{N}(F^*)^{k-j} = \{F^* - (F^*)^{N-j+1}\}/(1 - F^*) \quad (15)$$

where $\mathbf{d}_i$ is a displacement vector between the i and $i+1$ particles and F^* is the complex conjugate of F. $F(\mathbf{h})$ may be written as

$$F(\mathbf{h}) = \langle\exp\{-i(\mathbf{h}\cdot\mathbf{d}_i)\}\rangle = \int H_1(\mathbf{z})\exp\{-i(\mathbf{h}\cdot\mathbf{z})\}\,d\mathbf{z} \quad (16)$$

The function $H_1(\mathbf{z})$ is the probability of finding the nearest-neighbor particle at a displacement vector $\mathbf{z}$ and is represented by the function introduced by Hoseman.[26] The function is given in Appendix III. Carrying out the somewhat complicated calculations proposed by Hashimoto et al.,[25] we reduce eq 12b to

$$I(\mathbf{h},\alpha) = [\langle|f|^2\rangle + |\langle f\rangle|^2] + |\langle f\rangle|^2[Z_1(\mathbf{h},\alpha) + I_c(\mathbf{h},\alpha)/N] \quad (17)$$

where $Z_1(\mathbf{h},\alpha)$ and $I_c(\mathbf{h},\alpha)$ are described in Appendix IV. The scattered intensity $I = I(\mathbf{h},\alpha)$ in eq 17 and the particle scattering amplitude $f = f(h,\alpha,\xi)$ may be calculated for a given orientation α of the assembly or nucleus (OZ_2) axis and for a given orientation ξ of the sheaf (OZ_3) axis. Following Hashimoto et al.,[25] we consider two special cases, viz., (i) when the assemblies are oriented at a particular angle α_0 with respect to the stretching direction and there is no orientation disorder with respect to the assembly axis and the sheaf axis, and (ii) when the assemblies assume the same orientation as in case i but the sheaf axes have some independent orientation fluctuation. In the former case, eq 17 reduces to

$$I(\mathbf{h}) = CN|f(\mathbf{h},\alpha_0,\xi_0)|^2[Z_1(\mathbf{h},\alpha_0) + I_c(\mathbf{h},\alpha_0)/N] \quad (18)$$

In the latter case, eq 17 reduces to

$$I(\mathbf{h}) = CN\{\langle|f(\mathbf{h},\alpha_0,\xi_0)|^2\rangle - |\langle f(\mathbf{h},\alpha_0,\xi)\rangle|^2 + |\langle f(\mathbf{h},\alpha_0,\xi)\rangle|^2 \times [Z_1(\mathbf{h},\alpha_0) + I_c(\mathbf{h},\alpha_0)/N]\} \quad (19)$$

where

$$\langle|f(\mathbf{h},\alpha_0,\xi)|^2\rangle = \frac{\int_0^{2\pi} p_2(\xi)|f(\mathbf{h},\alpha_0,\xi)|^2\,d\xi}{\int_0^{2\pi} p_2(\xi)\,d\xi} \quad (20)$$

$$|\langle f(\mathbf{h},\alpha_0,\xi)\rangle|^2 = \left|\frac{\int_0^{2\pi} p_2(\xi)f(\mathbf{h},\alpha_0,\xi)\,d\xi}{\int_0^{2\pi} p_2(\xi)\,d\xi}\right|^2 \quad (21)$$

Under H_v polarization conditions, the total field $f(\mathbf{h},\alpha,\xi)$ from a sheaflike texture may be given by

$$f(\mathbf{h},\alpha,\xi) = f(\alpha,\xi) = C(1/2)(3\cos^2\omega_0 - 1)\int_{\pi/2-\gamma_0}^{\pi/2+\gamma_0}\sin[2(\alpha+\xi+\gamma)] \times \left[\frac{\sin\{-(2\pi R/\lambda)\sin\theta\cos(\alpha+\gamma+\xi-\mu)\}}{-(2\pi R/\lambda)\sin\theta\cos(\alpha+\gamma+\xi-\mu)} + \frac{\cos\{-(2\pi R/\lambda)\sin\theta\cos(\alpha+\gamma+\xi-\mu)\}}{\{-(2\pi R/\lambda)\sin\theta\cos(\alpha+\gamma+\xi-\mu)\}} + \frac{1}{\{-(2\pi R/\lambda)\sin\theta\cos(\alpha+\gamma+\xi-\mu)\}^2}\right] d\gamma \quad (22)$$

In this model system, the optical axes are fixed at a polar angle ω_0 with respect to the radial direction but randomly oriented around the radial direction. The derivation of eq 22 was carried out by using a method similar to that proposed by Clough et al.[28] $p_2(\xi)$ is, as proposed by Hashimoto et al.,[25] the orientation function for the sheaf axis and is given by

$$p_2(\xi) = \exp[-\sigma_\xi(\sin\xi - \sin\xi_0)^2] \quad (23)$$

The size distribution of the assembly or distribution of N in the assembly is also considered by assuming the distribution function $P(N)$,[29] which may be written as

$$P(N) = \exp\left[-\frac{(N-\bar{N})^2}{2\sigma_N^2}\right] \Big/ \sum_{N=1}^{2\bar{N}-1}\exp\left[-\frac{(N-\bar{N})^2}{2\sigma_N^2}\right] \quad (24)$$

where $\bar{N}$ and σ_N^2 are the average number of particles in the assembly and its standard deviation. Then the average zero-order scattering, $\langle I_c\rangle_{av}$, is given by

$$\langle I_c\rangle_{av} = \sum_{N=1}^{2N-1} I_c(N)P(N) \quad (25)$$

In actual calculation, the disorder in the interparticle distance is assumed to occur only along the assembly axis (OZ_2). The angle ω_0 in eq 22 is defined as 90° from the V_v scattering pattern in Figure 7a.

Figure 16 shows the light scattering patterns for an assembly of finite size, $\bar{N} = 10$. Pattern a is calculated without interparticle effects in the case where the Z_3 axis is parallel to the Z_1 axis. The scattering lobes show a maximum in the θ direction along the azimuthal angle of highest intensity and are extended in the stretching direction (i.e., the Z_1 axis), and this pattern closely resembles the ones observed at an extension ratio of $1.5 < \lambda < 2.3$ as shown in Figure 10. Pattern b is calculated by using

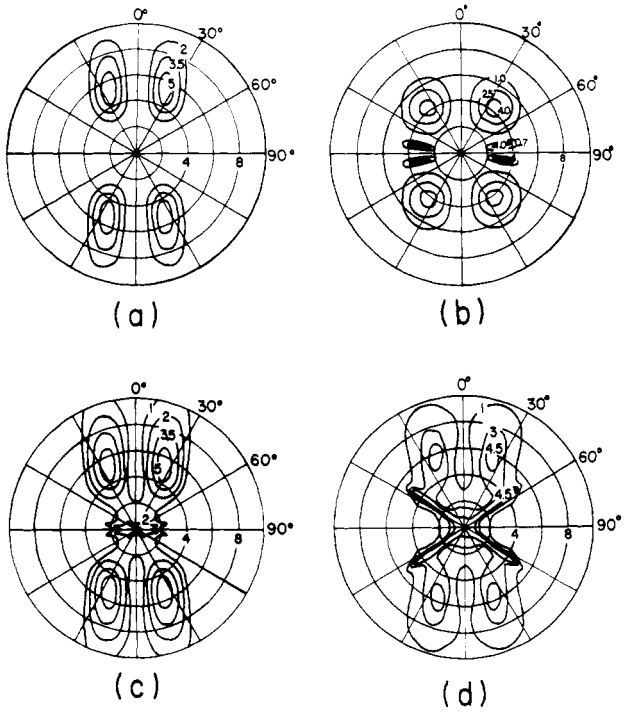

Figure 16. Calculated H_v scattering patterns for the following assemblies: (a) The assemblies with $\gamma_0 = 30°$ are perfectly oriented along the vertical direction. (b) The assemblies with $\gamma_0 = 45°$ are oriented at a particular angle ±8° and the sheaf axes are perpendicular to the z_1 axis. (c) The assemblies with $\gamma_0 = 30°$ are oriented at a particular angle ±8° but the sheaf axes have some orientation fluctuation with respect to the assembly axis. (d) The assemblies with $\gamma_0 = 30°$ are oriented at a particular angle ±35° but the sheaf axes have some orientation fluctuation with respect to the assembly axis.

eq 18 in the case when the assemblies are oriented at a particular angle $\alpha_0 = 8°$ and the sheaf axis is perpendicular to the Z_1 axis. That is, it corresponds to case i. This scattering pattern shows broad four-leaf lobes extended in the stretching direction at small azimuthal angles and sharp narrow four-leaf streaks at large azimuthal angles. The four streaks are, as a whole, attributed to the assemblies that are oriented preferentially at a particular angle α_0 with respect to the stretching direction. This pattern is close to the ones observed at extension ratios between $\lambda = 2.7$ and $\lambda = 4.0$. Patterns c and d are calculated by using eq 19, which corresponds to case ii. That is, the sheaf axes have some orientation fluctuations within the assemblies oriented at a particular angle α_0 with respect to the stretching direction. The values of α_0 are given as 8° and 35°, respectively. The pattern calculated at $\alpha_0 = 35°$ is rather close to the one observed at $\lambda = 2.5$.

The good agreement between the observed and calculated patterns indicates row-nucleated sheaves composed of branched lamellar overgrowth. The lamellar branching arises predominantly perpendicular to the stretching direction. This may be deduced from the four scattering lobes whose elongation in the stretching direction increases with extension ratio λ. This tendency, as discussed earlier in this paper, is connected with an increase in the degree of crystallinity. With a further increase of extension ratio, the lamellar branching seems to increase, as suggested by the increase of crystallinity shown in Figure 12. In this process, it may be postulated that rows of nucleating points assume specific orientations at a particular angle with respect to the stretching direction. However, we must recognize that this characteristic arrangement of sheaves involves, more or less, orientational disorder. Thus, the assemblies of sheaflike textures must be arranged with some orientational disorder in terms of orientation of the assembly axis and the sheaf axis. This disorder decreases with increasing degree of crystallinity and with decreasing values of α_0 as the film is further elongated. Beyond $\lambda = 2.7$, the scattering lobes become broader and the pattern closely resembles a four-leaf-clover type. It seems as though the aperture angle $2\gamma_0$ increases due to the increase of lamellar growth. This means that the sheaflike texture becomes close to a spherulitic texture. The pattern beyond the extension ratio $\lambda = 4.5$ becomes small and its scattered intensity becomes very weak. This implies that the transformation from the sheaves to fibrillar structures is due to the lamellar overgrowths disintegrating into small lamellar fragments.

IV. Conclusion

The deformation mechanism of PET under uniaxial stretching was investigated. Two kinds of specimens were used. One was of about 43% crystallinity and was stretched at 90 °C. The orientation was evaluated in terms of the second-order orientation factors of the three crystallographic axes and of amorphous chain segments. The orientation factors for the crystallographic axes were obtained from the orientation factors of the five crystal planes $(0\bar{1}1)$, (010), $(\bar{1}10)$, (100), and $(1\bar{1}1)$. The orientation of the amorphous chain segments was obtained by subtracting the crystalline contribution from the total birefringence, the calculation being carried out by assuming random rotation around the amorphous chain segments. The crystal *c* axes assumed preferential orienation in the stretching direction and this tendency became pronounced with increasing extension ratio. At an extension ratio of $\lambda = 2.0$, the amorphous chain segments also assumed preferential orientation but the orientational degree was not so pronounced as that of the crystal *c* axes. By contrast, with further elongation up to $\lambda = 3.8$ the amorphous chain segments attained considerable preferential orientation and the orientational degree was much more effective than that of the crystal *c* axes. Moreover, the light scattering patterns were accounted for by an affine deformation mode of spherulites that has been usually observed for crystalline polymers.

The other specimen was amorphous PET with about 3% crystallinity and was preheated at 95 °C for about 15 min and stretched at the same temperature. The scattering lobes of the H_v scattering pattern were elongated in the stretching direction up to $\lambda = 2.7$. With further increases of the extension ratio, the scattering pattern showed a broad four-leaf lobe pattern at small azimuthal angles and a sharp narrow four-leaf streak pattern at large azimuthal angles. These changes of the patterns were different from the results for the specimen with 43% crystallinity. The difference is due to the mechanism of crystallization under uniaxial stretching. The sequence of scattering patterns with increase of extension ratio may be analyzed by assuming the existence of a row-nucleated sheaflike structure in which the rows are preferentially oriented at a particular angle with respect to the stretching direction. The theoretical patterns were close to the observed ones. This indicates that the row-nucleated assemblies arising from branched lamellar overgrowths are oriented at a particular angle with respect to the stretching direction. This characteristic orientation was associated with an increase in the observed crystallinity and birefringence.

Acknowledgment. We thank Professor Kawai, Department of Polymer Chemistry, Faculty of Engineering, Kyoto University, Japan, for valuable comments and suggestions. Thanks are also due to Dr. Inoue and Mr.

Motegi, Film Division, Toray Industries, Inc., for the sample used. We are also grateful to Dr. R. St. John Manley, Department of Chemistry, McGill University, for his kind help with the English presentation.

Appendix I

According to the method of Roe,[14] the orientation factor of the jth crystal plane, A_m^j, is given by

$$A_{lm}^{j} = (2\pi)\left\{\frac{2}{2l+1}\right\}^{1/2} \times \sum_{n=-l}^{l} [A_{lmn} \cos n\Phi_j - B_{lmn} \sin \Phi n_j]\Pi_l^n(\cos \Theta_j) \quad \text{(A1)}$$

where $\Pi_l^n(\cos \Theta_j)$ is the normalized associated Legendre polynomial and A_{lmn} and B_{lmn} are the coefficients that are given by the series expansion of the crystallite orientation. Now let us consider the following orthogonal biaxial symmetry of the orientation distribution function $q_j(\cos \vartheta_j,\phi_j)$ of the reciprocal lattice vector U_j of the jth crystal plane. Equation A1 is simplified as

$$A_{lm}^{j} = (2\pi)\left\{\frac{2}{2l+1}\right\}^{1/2} \{A_{lm0}\Pi_l(\cos \Theta_j) + 2\sum_{m=1}^{l} (A_{lmn} \cos n\Phi_j - B_{lmn} \sin n\Phi_j)\Pi_l^n(\cos \Theta_j)\} \quad \text{(A2)}$$

For the uniaxially oriented system with respect to the X_3 axis, eq A-2 reduces to

$$A_{l0}^{j} = (2\pi)\left\{\frac{2}{2l+1}\right\}^{1/2} \{A_{l00}\Pi_l(\cos \Theta_j) + 2\sum_{n=1}^{l} (A_{l0n} \cos n\Phi_j - B_{l0n} \sin n\Phi_j)\Pi_l^n(\cos \Theta_j)\} \quad \text{(A3)}$$

The coefficients A_{l0}^j, A_{l0n}, and B_{l0n} may be considered as a sort of orientation factor, i.e., an average degree of orientation distribution. Therefore one can define the generalized orientation factors as follows:

$$F_{l0n} = \left\{\frac{2}{2l+1}\frac{(l+n)!}{(l-n)!}\right\}^{1/2} 4\pi^2 A_{l0n}$$

$$G_{l0n} = \left\{\frac{2}{2l+1}\frac{(l+n)!}{(l-n)!}\right\}^{1/2} 4\pi^2 B_{l0n}$$

$$F_{l0}^{j} = \left\{\frac{2}{2l+1}\right\}^{1/2} 2\pi A_{l0}^{j} \quad \text{(A4)}$$

Substituting eq A4 into eq A3, we may rewrite eq A3 as follows:

$$F_{l0}^{j} = F_{l00}P_l(\cos \Theta_j) + 2\sum_{n=1}^{l} \frac{(l-n)!}{(l+n)!}(F_{l0n} \cos n\Phi_j - G_{l0n} \sin n\Phi_j)P_l^n(\cos \Theta_j) \quad \text{(A5)}$$

where $P_l^m(x)$ and $P_l(x)$ are the associated Legendre polynomial and Legendre polynomial, respectivley (not normalized). In the case of $l = 2$, eq A5 reduces to eq 2.

Appendix II

The H_v scattered amplitude from a two-dimensional spherulite with the optical axes lying in the plane of the spherulite is given by

$$E = KN' \int_0^{2\pi} \int_0^{R'} (\mathbf{M}\cdot\mathbf{O}) \cos [k(\mathbf{r}'\cdot\mathbf{s})]r'\, dr'\, d\alpha' \quad \text{(A6)}$$

$$E = KN_0 \int_0^{2\pi} \int_0^{R'} (\mathbf{M}'\cdot\mathbf{O}) \cos [k(\mathbf{r}'\cdot\mathbf{s})]r\, dr\, d\alpha \quad \text{(A7)}$$

where $\mathbf{M}'\cdot\mathbf{O}$ denotes the vector product of the induced dipole moment $\mathbf{M}'$ and the vector $\mathbf{O}$ along the polarization direction of the analyzer for the horizontal polarization; assuming an affine organization of the optical axes, $\mathbf{M}'\cdot\mathbf{O}$ is given by

$$\mathbf{M}'\cdot\mathbf{O} = E_0\delta_0 \frac{\sin (\alpha + \omega_0) \cos (\alpha + \omega_0)}{\lambda_2 \sin^2 (\alpha + \omega_0) + \lambda_3 \cos^2 (\alpha + \omega_0)} \quad \text{(A8)}$$

where E_0 is the field strength of the incident beam and δ_0 is the anisotropy of the scattering element defined by $\alpha_\parallel - \alpha_\perp$, which is assumed to be uniaxially symmetrical with polarizabilities $\alpha_\parallel$ and $\alpha_\perp$ along and perpendicular to the optical axis. N_0 and N' are the densities of scattering material for the undeformed and deformed spherulites, respectively. λ_3 and λ_2 are the extension ratios parallel and perpendicular to the stretching directions, respectively. The angular coordinates of the radial vectors $\mathbf{r}$ and $\mathbf{r}'$ to a given scattering element are (r, α) within an undeformed spherulite and (r', α) within a deformed one. The vector $\mathbf{s}$ is given as $\mathbf{s}_0 - \mathbf{s}'$, where $\mathbf{s}_0$ and $\mathbf{s}'$ are unit incident and scattered ray vectors. The term $\cos [k(\mathbf{r}'\cdot\mathbf{s})]$ was given by Clough et al.[28] in the case where the spherulite deforms according to an affine mode.

Appendix III

As discussed by Hashimoto et al.,[25] the function $H_1(\mathbf{z})$ denoting the distance statistic is represented as the H-function introduced by Hoseman,[27] which may be given by

$$H_1(\mathbf{z}) = (2\pi)^{-3/2}(\Delta d_{zx}\Delta d_{zy}\Delta d_{zz})^{-1/2} \times \exp\left\{-\frac{1}{2}\left[\frac{x_2^2}{\Delta d_{zx}^2} + \frac{y_2^2}{\Delta d_{zy}^2} + \frac{(z-\bar{d})^2}{\Delta d_{zz}^2}\right]\right\} \quad \text{(A9)}$$

where $\bar{d}$ is the average distance between adjacent particles and $\bar{d}_{zi}$ is the average fluctuation of the displacement vector $\bar{d}_i$ between the two adjacent particles in the ith distance ($i = x_2$, y_2, and z_2 axes). If there is no fluctuation of the displacement in the direction of the x_2 and y_2 axes, eq A9 reduces to

$$H_1(\mathbf{z}) = (2\pi\Delta d_{zz}^2)^{-1/2} \exp[-(z_2 - d)^2/(2\Delta d_{zz}^2)] \quad \text{(A10)}$$

$$H_1(\mathbf{z}) = (2\pi\Delta d^2)^{-1/2} \exp[-(z_2 - d)^2/(2\Delta d^2)] \quad \text{(A11)}$$

The calculation in this paper was carried out by using eq A11.

Appendix IV

$Z_1(\mathbf{h})$ and $I_c(\mathbf{h})$ were derived by Hashimoto et al.[25] and are given as follows:

$$Z_1(\mathbf{h}) = Z_1(\mathbf{h},\alpha) = \text{Re}\,[(1+F)/(1-F)] = [1 - |F|^2]/[1 + 2|F| \cos (\mathbf{h}\cdot\mathbf{d}) + |F|^2] \quad \text{(A12)}$$

and

$$I_c(\mathbf{h}) = I_c(\mathbf{h},\alpha) = -2\,\text{Re}\,[F(1-F^N)/(1-F)^2] = 2|F|\{[1 + |F|^2] \cos (\mathbf{h}\cdot\mathbf{d}) - 2|F| - |F|^N \times \cos [(N+1)(\mathbf{h}\cdot\mathbf{d})] + 2|F|^{N+1} \cos [N(\mathbf{h}\cdot\mathbf{d})] - |F|^{N+2} \times \cos [(N-1)(\mathbf{h}\cdot\mathbf{d})]\}[1 - 2|F| \cos (\mathbf{h}\cdot\mathbf{d}) + |F|^2] \quad \text{(A13)}$$

References and Notes

(1) Ward, I. M. *Text. Res. J.* **1961**, *31*, 650.
(2) Dulmage, W. J.; Geddes, A. L. *J. Polym. Sci.* **1958**, *15*, 499.
(3) Farrow, G.; Bagley, J. *Text. Res. J.* **1962**, *32*, 587.
(4) Heffelfinger, C. J.; Schmidt, P. G. *J. Appl. Polym. Sci.* **1965**, *9*, 2261.
(5) Dumbleton, J. H.; Bowles, B. B. *J. Polym. Sci., Part A-2* **1966**, *4*, 951.
(6) Wallach, M. L. *J. Polym. Sci., Part C* **1966**, *13*, 69.
(7) Yoshioka, N.; Sato, H. *Kobunshi Kagaku* **1969**, *26*, 486.

(8) Konda, A.; Nose, K.; Ishikawa, H. *J. Polym. Sci., Polym. Phys. Ed.* **1976**, *14*, 1495.
(9) Misra, A.; Stein, R. S. *J. Polym. Sci., Polym. Phys. Ed.* **1979**, *17*, 235.
(10) Bosley, D. E. *J. Appl. Polym. Sci.* **1964**, *8*, 1521.
(11) de Daubeny, R.; Bunn, C. W.; Brown, C. J. *Proc. R. Soc. London, Ser. A* **1954**, *226*, 531.
(12) Roe, R.-J.; Krigbaum, W. R. *J. Chem. Phys.* **1964**, *40*, 2608.
(13) Krigbaum, W. R.; Roe, R.-J. *J. Chem. Phys.* **1964**, *41*, 737.
(14) Roe, R.-J. *J. Appl. Phys.* **1965**, *36*, 2024.
(15) Krigbaum, W. R.; Balta, Y. I. *J. Phys. Chem.* **1967**, *71*, 1770.
(16) Matsuo, M.; Hirota, K.; Fujita, K.; Kawai, H. *Macromolecules* **1978**, *11*, 1000.
(17) Matsuo, M.; Ozaki, F.; Kurita, H.; Sugawara, S.; Ogita, T. *Macromolecules* **1980**, *13*, 1187.
(18) Stein, R. S.; Norris, F. H. *J. Polym. Sci.* **1956**, *21*, 381.
(19) Bunn, C. W.; de Daubeny, R. *Trans. Faraday Soc.* **1954**, *50*, 1173.
(20) Sakaguchi, N.; Oda, T.; Nakai, A.; Kawai, H. *Seni-Gakkaishi* **1977**, *33*, 779.
(21) Samuels, R. J. *J. Polym. Sci., Part C* **1966**, *13*, 37.
(22) van Aartsen, J. J.; Stein, R. S. *J. Polym. Sci., Part A-2* **1971**, *9*, 295.
(23) Motegi, M.; Oda, T.; Moritani, M.; Kawai, H. *Polym. J.* **1970**, *1*, 209.
(24) Picot, C.; Stein, R. S.; Motegi, M.; Kawai, H. *J. Polym. Sci., Part A-2* **1970**, *8*, 2115.
(25) Hashimoto, T.; Todo, A.; Kawai, H. *Polym. J.* **1978**, *10*, 521.
(26) Hoseman, R.; Bagchi, S. N. "Direct Analysis of Diffraction by Matter"; North-Holland Publishing Co.: Amsterdam, 1962.
(27) Hashimoto, T.; Todo, A.; Murakami, Y.; Kawai, H. *J. Polym. Sci., Polym. Phys. Ed.* **1977**, *15*, 501.
(28) Clough, S.; van Aartsen, J. J.; Stein, R. S. *J. Appl. Phys.* **1965**, *36*, 3072.
(29) Hashimoto, T.; Nagatoshi, K.; Todo, A.; Hasegawa, H.; Kawai, H. *Macromolecules* **1974**, *7*, 364.

Oriented Crystallization of Poly(ethylene terephthalate) under Uniaxial Stretching

Takako Terada,† Chie Sawatari, Toyoko Chigono, and Masaru Matsuo*

Department of Clothing Science, Faculty of Home Economics, Nara Women's University, Nara 630, Japan. *Received February 24, 1982*

ABSTRACT: The deformation behavior of poly(ethylene terephthalate) films was investigated in terms of orientation of the amorphous chain segments and deformation of superstructures by using small-angle light scattering and birefringence techniques. The elongation was done in a hot air oven and in a hot water bath at different temperatures. The orientation of the amorphous chain segments increased considerably with decreasing elongation temperature. From this it is concluded that the mobility of the polymer chains increases with increasing temperature and, therefore, the amorphous regions stretched at lower temperature behave like paracrystallites. This phenomenon was well accounted for by the results calculated on the basis of a model proposed by Roe and Krigbaum concerning the orientation distribution of statistical segments in deformed networks. Differential scanning calorimetry experimental results supported the temperature dependence of the mobility of the polymer chains. Light scattering patterns at lower extension ratios showed four-leaf lobes extended in the direction of stretching having a maximum in the polar direction along the azimuthal angle of highest intensity. With increasing extension ratios, the scattering exhibited multilobed patterns having sharp narrow four-leaf streaks in addition to the lobes. The appearance of the streak depended on the crystallinity of the film, which is affected by the elongation temperature. These results indicate that the orientation and deformation of sheaflike textures are associated with oriented crystallization. In addition, the shrinkage of bulk specimens was profoundly affected by the crystallinity.

Introduction

In the previous paper,[1] the deformation mechanism of poly(ethylene terephthalate) (PET) was investigated both theoretically and experimentally in terms of the molecular orientation and superstructural deformation by means of small-angle light scattering, X-ray diffraction, and birefringence techniques. These studies showed that the deformation mechanism is affected by the crystallinity of the undrawn specimens. When an undrawn film with a high degree of crystallinity (about 43% crystallinity) was stretched, the specimen showed almost a constant value of crystallinity under uniaxial stretching; the H_v light scattering pattern had four lobes extended in the horizontal direction and showed a maximum in the polar direction along the azimuthal angle of highest intensity. The deformation was therefore accounted for by a spherulitic model with an affine deformation. On the other hand, when an amorphous film (about 3% crystallinity) was stretched, the crystallinity increased with increasing extension ratio. The H_v scattering showed a broad four-leaf lobe pattern at small azimuthal angles and a sharp narrow four-leaf streak pattern at large azimuthal angles. The analysis was carried out by comparing the theoretical and observed patterns. The agreement between the calculated and observed patterns suggested the occurrence of crystallization associated with the existence of row-nucleated sheaflike textures whose rows are preferentially oriented at a particular angle with respect to the stretching direction.

In order to provide more conclusive evidence about the oriented crystallization, we investigated the deformation of the amorphous PET film in terms of the relation between crystallinity and scattering pattern as well as in terms of the relation between the shape of differential scanning calorimetry (DSC) curves and the second-order orientation factor of the amorphous chain segments. The investigation was further extended to shrinkage mechanisms of bulk specimens.

Experimental Section

Samples were prepared from 385-μm amorphous PET films obtained through the courtesy of the Film Division of Toray Industries, Inc., Siga. The density of these films measured by a pycnometer, with *n*-heptane–carbon tetrachloride as a medium, was found to be 1.338 g/cm^3. Elongation was done under two

† Present address: Tamaki Women's College.

0024-9297/82/2215-0998$01.25/0